Chapter 5 : Configurational entropy stabilized NiMnSb and NiMnSbV medium-entropy alloy through high-energy ball milling

5.1 Introduction

High/medium entropy alloys have been investigated extensively over the last decade pertaining to its enhanced properties [140–144], which is otherwise difficult to achieve in conventional alloys. High-entropy ceramics is of relatively recent vintage [145–147] and these materials also show promising functional properties. Although the field started with high- entropy alloys, now a days it is a special class of materials known as high-entropy materials [148,149]. Initially, high-entropy alloys used to be defined as single-phase solid solution with five or more elements in almost equi-atomic ratios. In spite of extensive investigation, only a limited number of alloys have been discovered till date to form single-phase solid solution [150–153]. As of today, multiphase alloys are also termed as high/medium entropy alloys [154–156]. Additionally, the microstructure evolution and thermal stability of the phases in the microstructure is far from understood.

The term “high-entropy” originates from the existence of five or more elemental species in the same crystal lattice of solid solution or intermetallic phase. Due to the presence of five or more elements in the lattice, the number of configurational states is always more than 1.5R [157]. Due to the presence of large number of configurational states, the phase is believed to be always entropy stabilized irrespective of its enthalpy of formation [158,159]. However, considerable departure from this theory is observed in practice. A supposedly entropy stabilized phase at ambient temperature shows phase transformation upon moderate to high temperature exposure for a suitable length of time. Wu et al. [160] have showed increased damping capacity of Ti-Zr-Hf-Co-Cu-Ni alloy, and this enhanced property has been attributed to the configurational entropy along with high uneven internal stress and severe lattice distortion. Sun et al. [161] have reported the formation of tetragonal Heusler alloys where the increased configurational entropy helps in increasing the Seeback coefficient of the alloy. However, Shivam et al. [162] have shown the formation of single-phase solid solution high-entropy alloy through

high-energy ball milling and the same composition with varied atomic percent, when cast through induction melting, showed two phase microstructure (BCC +B2) medium-entropy alloy. Detailed composition analysis upon heat treatment of this alloy, shows continuous variation in the composition of the two phases and a segregation of different elemental species in different phases. As the high entropy stabilization is often questioned and debated, this class of alloys are also termed as multicomponent alloys or complex-concentrated alloys.

Several processing routes have been adopted to synthesize high entropy alloys i.e. high energy ball milling, solidification of a melt etc. Mechanical milling or mechanical alloying has gained traction over past 3-4 decades as equilibrium, non-equilibrium and amorphous phases could be synthesized using this process [67,73]. This non-equilibrium processing results in the extension of solid solubility of immiscible elements having distinct melting temperatures, and often twiddling the process parameters leads to the formation of intermetallics, quasicrystals or amorphous phases [163]. The extension of solid solubility of Sn in FeCo system has been investigated by Loureiro et al. [164], where they have reported the formation of disordered BCC solid solution through mechanical milling. Formation of quasicrystals through mechanical alloying coupled with spark plasma sintering has also been observed in Al-Ni-Co alloys, where decagonal quasicrystals with periodicity in one direction and quasi-periodicity in the other two directions is observed [165]. Al-Cu-Fe forms an icosahedral quasi-crystalline phase after mechanical alloying, which has many interesting catalytic properties [166], Ti-Zr-Ni-Co alloy also forms an icosahedral quasicrystals by mechanical alloying, which can be used for hydrogen storage [167]. Formation of amorphous phase through mechanical alloying has also been observed for many alloy systems [168], amorphization of Zr alloy has been observed for the first time by Helistern and Schultz by mechanical alloying [169]. Adamzadeh et al. [170] have also employed the mechanical alloying method to fabricate an amorphous coating of Ni-Nb alloys.

The present study is aimed at understanding the phase and microstructure evolution in NiMnSb semi-Heusler and vanadium (V) added NiMnSbV alloy through mechanical alloying. The same alloys synthesized through solidification route has been studied and given in chapter 4 [171]. It has been observed that NiMnSb alloy forms single-phase semi-Heusler intermetallic in the alloy. However, the NiMnSbV alloy

additionally forms Frank-Kasper SbV_3 phase along with the semi-Heusler NiMnSb phase. A comparison of the phase evolution and microstructure in these alloys through mechanical alloying and solidification would help in deciphering the processing route dependence of phase and microstructure evolution in these alloys.

5.2 Experimental Techniques

The high purity (Alfa Aesar,99.5 % purity) elemental powders of Ni, Mn, Sb and V with ~325 mesh has been used for this study. The elemental powders of Ni, Mn, Sb and V (weighing ~40 g) were taken in equi-atomic proportion and were pre-mixed for alloying. The high energy planetary ball mill (Retsch PM 400) operated at 200 rpm was used for mechanical alloying (MA) of pre-mixed powders. The powder was placed in tungsten carbide (WC) vials (250 ml) with~10 mm diameter WC balls. The ball to powder ratio (BPR) was kept at 10:1, and milling was carried out in wet condition using toluene as process control agent to avoid overheating and oxidation. The milling was intermittently stopped after every 2 h of milling for 1 h to control the rise in temperature during mechanical alloying. For discerning the alloying behaviour and phase evolution during milling, small amount (~2-3 g) of milled powder was extracted at regular intervals of 10 h, 40 h, 70 h, and 100 h.

X-ray diffraction (XRD) experiments were performed using a Rigaku Mini Flex 600 with CuK_α radiation (~1.543 Å) with 40 kV accelerating voltage and 15 mA tube current. Samples were scanned from 10° to 90°, with a step size of 0.01° and scan rate of 5°/min. The scanning electron microscopy was carried out using a Quanta 200F in backscattered electron mode operated at 20kV. The nominal chemical compositions of the as-cast samples were investigated by SEM equipped with X-ray energy dispersive spectrometer (EDS). The powder was suspended in ethanol and it was ultra-sonicated for 15 minutes before it was drop cast onto a carbon coated copper grid. The fine structural and microstructural details of the alloyed MEAs were ascertained through transmission electron microscopy using a TECNAI G^2 T20 (LaB_6 filament) TEM operating at 200 kV in diffraction contrast and Nano-beam electron diffraction (NBED) modes.

5.3 Results

The NiMnSb and NiMnSbV MEAs were mechanically alloyed up to 100 h. The alloying behavior and phase evolution during alloying was monitored through XRD. Multiple display of x-ray diffraction patterns of NiMnSb and NiMnSbV MEAs milled for 10 h, 40 h, 70 h and 100 h are shown in Figure 5.1 (a) and 5.1 (b) respectively. In NiMnSb system (Figure 5.1(a)) after 10 h of mechanical alloying, distinct peaks of hexagonal (Ni/Mn)Sb phase (Pearson symbol: hP4, SG: $P6_3/mmc$ and a = b = 4.149Å, c = 5.771 Å) is observed. Along with the hexagonal (Ni/Mn)Sb phase, some additional peaks are also observed, which cannot be indexed to any known phase. However, the additional peaks at 31.3°, 44.1°, 45.7°, 56.4°, 58.8° and 60.6° can be indexed to a newly formed disordered hexagonal solid solution phase (SG: $P6_3/mmc$ and a = b = 3.97Å, c = 5.12 Å, c/a=1.28). On continued alloying, after 40 h of milling, the peak intensities of hexagonal (Ni/Mn)Sb phase reduces drastically and considerable peak broadening is observed. However, the peaks corresponding to the hexagonal solid solution phase continue to grow without any change in the peak position. This clearly indicates that the disordered hexagonal solid solution phase grows at the expense of the hexagonal (Ni/Mn)Sb phase. Strain accumulation and particle size refinement is evident from the peak broadening of the (Ni/Mn)Sb phase. After 70 h of alloying, the peaks corresponding to the hexagonal (Ni/Mn)Sb phase completely disappears indicating its complete dissolution. The peaks corresponding to the disordered hexagonal solid solution phase grow further without any change in the peak positions. After 100 h of alloying, the disordered hexagonal solid solution phase remains to be the only existing phase. However, the peaks are quite broad, which could be indicative of accumulated strain and refined particle size. There could be some amorphous phase also present, which will require confirmation through TEM.

Multiple display of X-ray diffraction patterns after different milling durations i.e. 10 h, 40 h, 70 h and 100 h for NiMnSbV system is given in Figure 5.1(b). In this system also after 10 h of mechanical alloying, distinct peaks of hexagonal (Ni/Mn)Sb phase along with the peaks for the disordered hexagonal solid solution phase could be observed. After 40 h of mechanical alloying, the peak intensities of the hexagonal (Ni/Mn)Sb phase reduces drastically and the peak intensities of the disordered hexagonal solid solution phase grows. Unlike the NiMnSb system, in the NiMnSbV

system, the hexagonal (Ni/Mn)Sb phase does not dissolve after 70 h of mechanical alloying. After 100 h of mechanical alloying, the presence of hexagonal (Ni/Mn)Sb phase could not be detected, all the diffraction peaks could be indexed to the disordered hexagonal solid solution phase (SG: $P6_3/mmc$ and a = b = 3.97Å, c = 5.12 Å, c/a=1.28). In this system also, the diffraction peaks are quite broadened, which points to the strain accumulation in the lattice, refined particle size and the probable presence of amorphous phase. The presence of amorphous phase needs to be confirmed by TEM. The phase evolution in NiMnSbV system remains to be similar to the NiMnSb system. However, phase formation kinetics in NiMnSbV is slower than the NiMnSb as it has been observed that the hexagonal (Ni/Mn)Sb phase dissolves in ~100 h of mechanical alloying to form the disordered hexagonal solid solution phase.

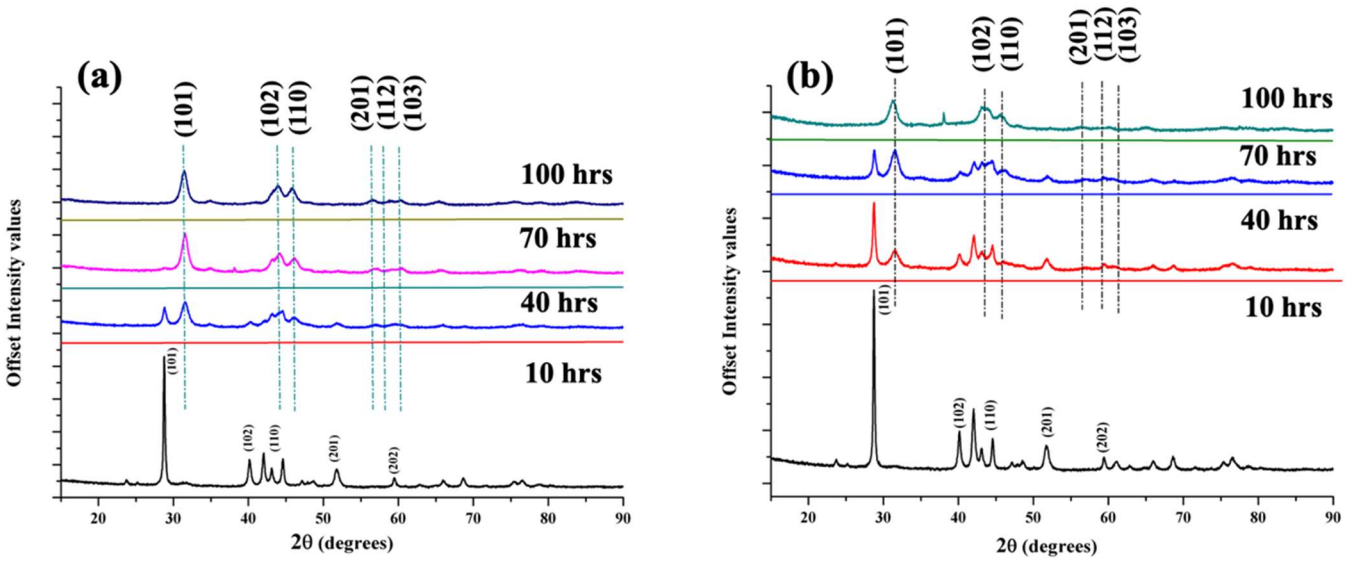

Figure 5.1: (a) Multiple display of X-ray diffraction patterns of mechanically alloyed Ni, Mn, Sb powders after 10 h, 40 h, 70 h and 100 h (b) Multiple display of X-ray diffraction patterns of mechanically alloyed Ni, Mn, Sb, V after 10 h, 40 h, 70 h and 100 h.

Simulated powder X-ray diffraction pattern in Figure 5.2(b) for the disordered hexagonal solid solution phase (SG: $P6_3/mmc$ and a = b = 3.97Å, c = 5.12 Å, c/a=1.28) in NiMnSb along with the experimental X-ray diffraction patterns for the same alloy after alloying for 10h, 40h, 70h and 100h is given in Figure 5.2(a). The diffraction peak

positions and the intensity profile in the experimental and simulated patterns brings out a good fit. This further confirms the formation of single phase disordered hexagonal solid solution in NiMnSb system after 100 h of mechanical alloying.

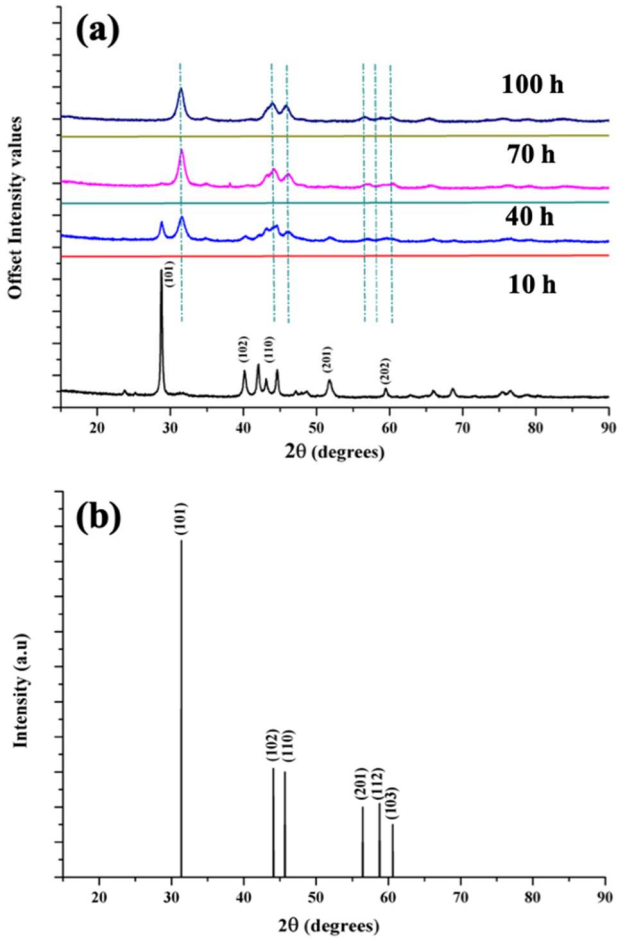

Figure 5.2: (a) Multiple display of X-ray diffraction patterns of mechanically alloyed Ni, Mn, Sb powder after milling for 10 h, 40 h, 70 h and 100 h. (b) Simulated X-ray diffraction pattern of newly formed disordered hexagonal phase showing a good match with the experimental pattern.

The crystallite size and crystallite strain of mechanically alloyed NiMnSb and NiMnSbV powders is calculated against the mechanical alloying duration. Crystallite size and strain is calculated from the Williamson-Hall plot. It has been observed that the crystallite size of (Ni/Mn)Sb phase and the newly found hexagonal phase follows a declining trend, whereas the crystallite strain follows an increasing trend with respect to

the increasing mechanical alloying duration. The volume fraction of the newly phase formed has been calculated from integration of the area of (Ni/Mn)Sb from the x-ray diffraction peaks employing the non-linear Pseudo-Voigt function for the peak fitting. The (Ni/Mn)Sb phase follows a decreasing trend in terms of volume fraction, whereas the newly formed hexagonal phase shows an increasing trend in terms of volume fraction.

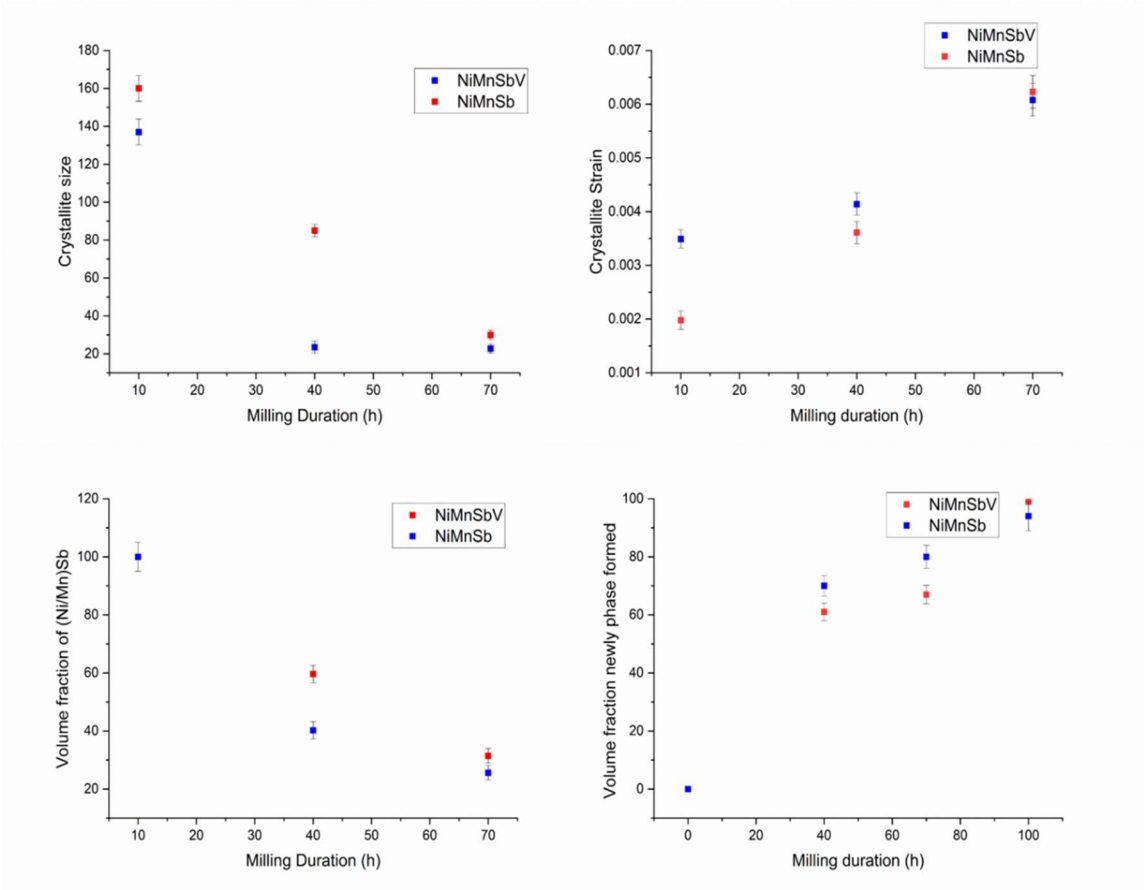

Figure 5.3 The graphs represent the variation of crystallite size, crystallite strain and volume fraction of the newly phase formed against the mechanical alloying duration.

The SEM micrographs of NiMnSb and NiMnSbV are displayed in Figure 5.4(a-h). Figure 5.4(a-d) shows the SEM micrograph of NiMnSb alloyed powders at different mechanical alloying durations (10 h, 40 h, 70 h, 100h). Similarly, for NiMnSbV alloyed powder, the SEM micrograph is displayed in Figure 5.4(e-h). The images were captured in the SE mode operating at 20 kV. The particle size reduction can clearly be seen with

respect to increasing mechanical alloying duration. The SEM micrographs in a way also justifies the results obtained from X-ray diffraction.

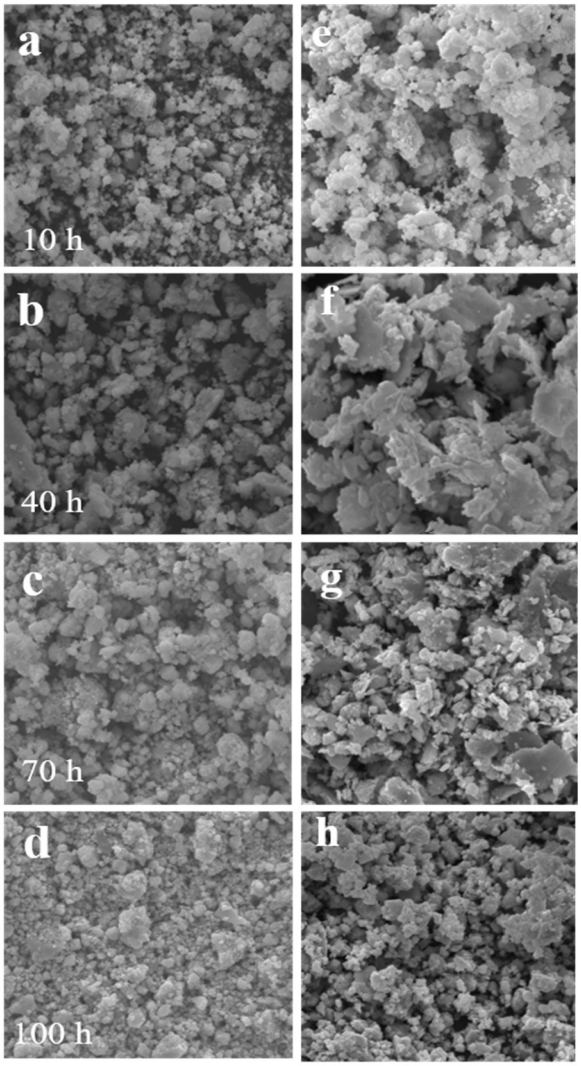

Figure 5.4 (a-d) The SEM micrographs of mechanically alloyed powders of NiMnSb and (e-h) NiMnSbV at different alloying duration .

TEM bright field images and corresponding electron diffraction patterns from different regions of the NiMnSb powder after mechanical alloying for 100 h are given in Figure 5.3(a-f). Presence of disordered hexagonal solid solution phase of NiMnSb could be confirmed from the bright field image in Figure 5.5(a) and the corresponding diffraction pattern in Figure 5.5(b). In the bright field image in Figure 5.5(a) strong crystallographic contrast of bend contours, dislocations and strain fields could be observed. The diffraction pattern in Figure 5.5(b) matches with z=[101]/[$2\bar{1}\bar{1}3$] zone

axis pattern of a disordered hexagonal phase. The lattice parameter of the disordered hexagonal solid solution phase as measured from the electron diffraction pattern matches quite closely with the same as measured from the powder x-ray diffraction pattern. The bright field image in Figure 5.5(c) shows the presence of

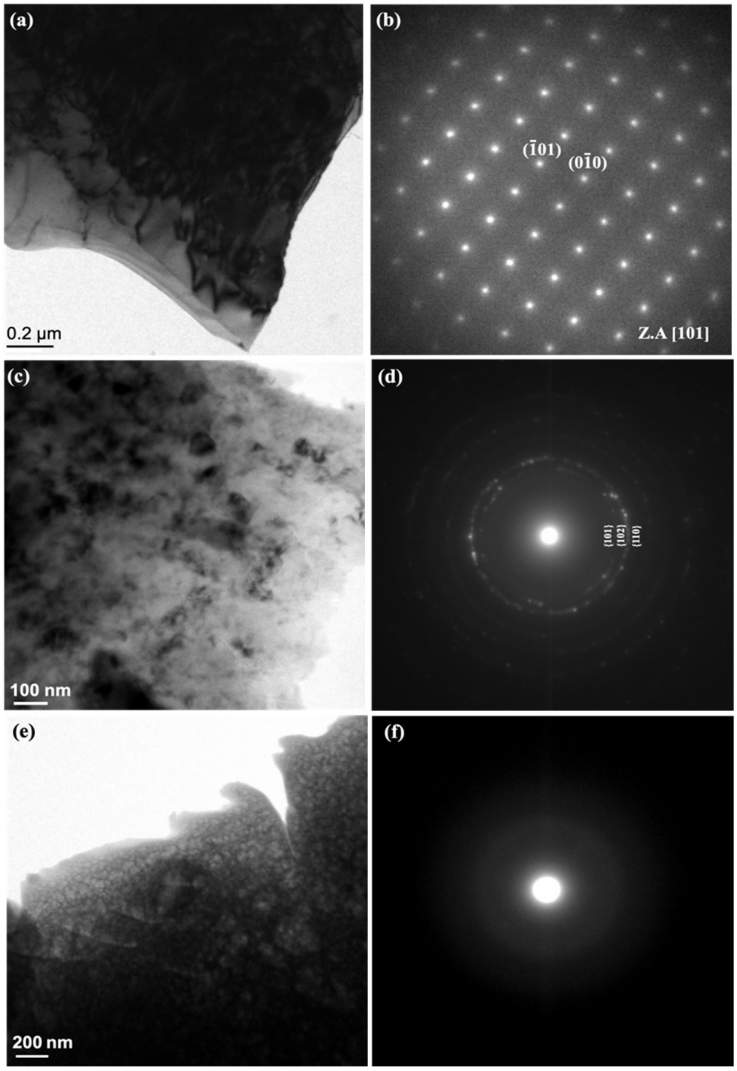

Figure 5.5 (a-f):TEM bright field images and corresponding electron diffraction patterns from different regions of the NiMnSb alloy after milling for 100 h. (a-b) Disordered hexagonal soilid solution phase with high dislocation density and the corresponding electron diffraction pattern along z=[101]. (c-d) Nanoparticles of disordered hexagonal solid solution phase embedded in the amorphous matrix and the corresponding electron diffraction pattern showing randomly oriented crystals. (e-f) Amorphous phase in the alloy with corresponding electron diffraction pattern represented by the diffused halo.

nanocrystalline NiMnSb phase. The size of the nanocrystals is ~30-50 nm and the presence of strain fields could easily be discerned. The corresponding diffraction pattern in Figure 5.5(d) shows a polycrystalline diffraction pattern. The Debye rings could be indexed to the standard hexagonal phase. The presence of the amorphous phase could be discerned from the bright field image in Figure 5.5(e) and the corresponding diffraction pattern in Figure 5.5(f). In the bright field image no crystallographic feature is observed and in the diffraction pattern a diffused halo indicative of the amorphous phase is present.

Bright field image and corresponding electron diffraction patterns from different regions of the equi-atomic NiMnSbV medium entropy alloy after 100 h of mechanical alloying are given in Figure 5.6(a-d). In the bright field image in Figure 5.6(a), nicely faceted particles of the size of ~100 nm is observed. The nano-beam electron diffraction pattern from one of the particles in Figure 5.6(b) brings out the hexagonal symmetry of the crystal (z=[0001]). In the bright field image from a different region of the same alloy in Figure 5.6(c), distribution of fine crystallites varying in the size range of ~10 nm is observed. The fine crystallites are embedded in the amorphous matrix. In the diffraction pattern from the same alloy in Figure 5.6(d) discontinuous Debye rings could be observed. The Debye rings can be indexed to the same newly formed disordered hexagonal phase. The presence of diffused halo in the diffraction pattern indicates the presence of amorphous phase in the alloy also.

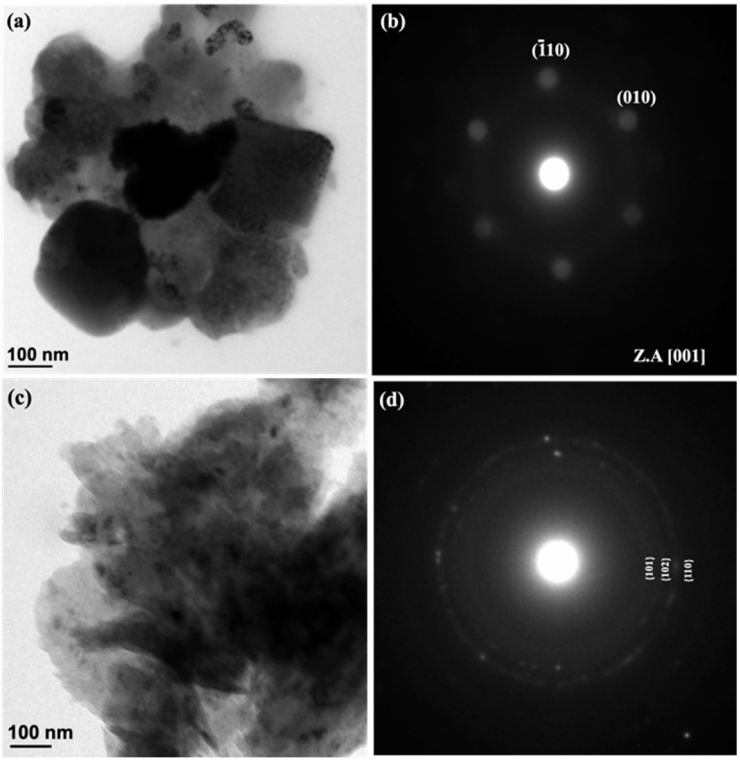

Figure 5.6(a-d) : TEM bright field images and corresponding electron diffraction patterns from different regions of the NiMnSbV alloy after milling for 100 h. (a) Cluster of faceted crystals of disordered hexagonal phase of NiMnSbV. (b) corresponding nano-beam electron diffraction pattern from one particle in (a) showing explicit 6-fold rotational symmetry from z=[001]/[0001] of the disordered hexagonal solid solution phase. (c) showing the presence of the amorphous phase with some embedded nanocrystals (d) corresponding electron diffraction pattern showing the amorphous phase as represented by the diffused halo and the disordered hexagonal phase as represented by the presence of the discontinuous Debye rings.

Scanning electron micrograph and XEDS spectra of induction melted and as-solidified NiMnSb and NiMnSbV alloy are given in Figure 4.2(a-d) respectively. In both the micrographs in Figures 4.2(a) and 4.2(c), solidification shrinkage porosities are observed. In the micrograph of the as-solidified NiMnSb in Figure 4.2(a) alloy no second phase is observed. XEDS spectra from this region in Figure 4.2(b) indicates to the uniform distribution of Ni, Mn and Sb in near equi-atomic proportion. In the micrograph from the as-solidified NiMnSbV alloy in Figure 4.2 (c), in addition to the

shrinkage porosities, two distinct phases are observed. The bright phase is semi Heusler NiMnSb with near equi-atomic distribution of Ni, Mn, Sb with minor quantities of V, whereas the dark phase is Frank-Kasper type SbV_3 phase with minor quantity of Ni and Mn, as observed from the XEDS spectra in Figure 4.2(d). In the interface region of the two phases, protrusions of SbV_3 phase into the semi Heusler NiMnSb phase leading to the formation of a lamellar structure is observed. The presence of protrusions indicates to the breakdown of the planar solidification front, solute segregation, the detailed mechanism of which would be discussed in the discussion section.

5.4 Discussion

The phase evolution in NiMnSb and NiMnSbV alloys as observed during mechanical alloying and after solidification, offers a comparative ground to understand the effect of processing route on phase evolution, configuration entropy stabilization effect in this alloy; and the role of atomic size mismatch and enthalpy of mixing in formation of single-phase medium entropy alloy. The important points are discussed in the following sections.

5.4.1 Processing route dependence of phase evolution

In this work, equi-atomic mixture of Ni, Mn, Sb and Ni, Mn, Sb and V powders were mechanically alloyed in wet medium to study the phase evolution. In case of Ni, Mn, Sb mixture, hexagonal (Ni/Mn)Sb ordered intermetallic phase forms after 10 h of alloying. With the progress of alloying duration, the hexagonal (Ni/Mn)Sb phase is destabilized to give birth to a disordered hexagonal solid solution phase of Ni, Mn and Sb. Complete destabilization of the hexagonal (Ni/Mn)Sb phase takes place after 70 h of mechanical alloying. In case of Ni, Mn, Sb and V mixture, the phase evolution sequence remains almost the same. However, complete destabilization of the hexagonal (Ni/Mn)Sb phase takes place after 100 h of mechanical alloying. The hexagonal (Ni/Mn)Sb phase appears in the phase diagram as a stable phase. However, continued mechanical alloying leads to the destabilization of the phase. It can be understood in the light of excessive strain that is imparted during mechanical alloying and the increase in configurational entropy while the ordered (Ni/Mn)Sb phase is destabilized to form disordered hexagonal solid solution phase. Thermodynamic aspect of this transformation will be discussed in the next section. In case of pure Ni, Mn, Sb mixture,

complete conversion to the disordered hexagonal phase takes place after 70 h of mechanical alloying and it takes about 100 h in case of Ni, Mn, Sb and V mixture. It can be concluded that V addition slows down the kinetics of phase transformation of the ordered hexagonal (Ni/Mn)Sb phase to disordered hexagonal solid solution phase. It may be presumably due to diffusion of V into the lattice of disordered hexagonal solid solution, which is an extra diffusion event that is required in NiMnSbV alloy in comparison to the NiMnSb alloy.

The NiMnSb alloy after solidification forms semi-Heusler NiMnSb phase and in the NiMnSbV alloy, blocky dispersion of Frank-Kasper type SbV_3 phase is observed in the matrix of semi-Heusler NiMnSb phase. The semi-Heusler NiMnSb phase is not stable beyond 400 ºC. It transforms to ordered hexagonal (Ni/Mn)Sb intermetallic phase. Phase evolution and thermal stability of the as-solidified alloy has been reported in chapter 4 [171]. In the as-solidified NiMnSbV alloy, at the interface of SbV_3 and semi-Heusler NiMnSb phase lamellar structure is observed. XEDS analysis from both the phases indicates that minor quantity of V is dissolved in semi-Heusler phase and minor quantity of Mn, Ni is dissolved in the SbV_3 phase. It may be deciphered from this observation that SbV_3 phase nucleates initially from the liquid melt and it rejects excess of Ni and Mn. The interface region of the SbV_3 phase becomes rich in Ni and Mn that leads the way for the nucleation of the hexagonal (Ni/Mn)Sb phase. While cooling below 800 ºC, the hexagonal (Ni/Mn)Sb phase transforms into semi-Heusler NiMnSb phase.

It is observed that the phase evolution sequence in NiMnSb and NiMnSbV alloys changes completely as the processing route is changed. In the as-solidified alloys, the NiMnSb semi Heusler phase is not stable beyond 400 ºC. Similarly, in the mechanically alloyed NiMnSb and NiMnSbV alloys the amorphous phase and the hexagonal solid solution phase remains to be metastable. It can be concluded from this observation that the phase evolution in medium-entropy NiMnSbV alloy remains to be processing route dependent. In the energy landscape of this alloy several local minima do exist, depending upon the processing route the alloy might get held up in one among the local minima. Upon imparting energy fluctuation from outside the alloy might land up in another local minimum or in a global minimum. In this regard, behavior of the

multicomponent medium-entropy alloys remains to be quite similar to the multicomponent bulk metallic glass forming alloys [137,172].

5.4.2 Effect of configurational entropy

It has been widely reported in high and medium-entropy alloy literature that in this class of alloys, presence of several elemental species increases the configurational entropy of the system as a result of which the free energy is always dominated by high configurational entropy irrespective of the enthalpy of mixing [148]. However, it has been observed in many such HEAs or MEAs multiple phases forms at ambient temperature, which essentially reduces the configurational entropy of the system [132]. Additionally, many of these phases undergo phase transformation upon medium to high temperature exposure [162]. In the present study, the NiMnSb and NiMnSbV alloys have been mechanically alloyed and the evolution of the single disordered hexagonal solid solution phase has been observed. The extent of disordering has been monitored through X-ray diffraction peak broadening and intensity calculation, which is given in Figure 5.7(a-b) for NiMnSb and NiMnSbV alloy powders respectively. In both the alloys, the highest intensity (101) peak of the ordered hexagonal (Ni/Mn)Sb phase has been monitored with the progress of mechanical alloying duration. For the NiMnSb alloy in Figure 5.7 (a) it is observed that the intensity of the (101) peak reduces drastically after 40 h of alloying signifying a disorder parameter s~0.37. For the NiMnSbV alloy in Figure 5.7(b), the kinetics of disordering becomes slower with a disordering parameter s~0.47 after 40 h of mechanical alloying and s~0.23 after 70 h of mechanical alloying. This observation is quite in line with the experimental observation. Additionally, continuous drop in the intensity and broadening of the profile with enhancement in serrated nature of the profile along with the flattening of the tail region indicates disordering along with severe strain induced defect formation during mechanical alloying. It increases the configurational entropy of the system.

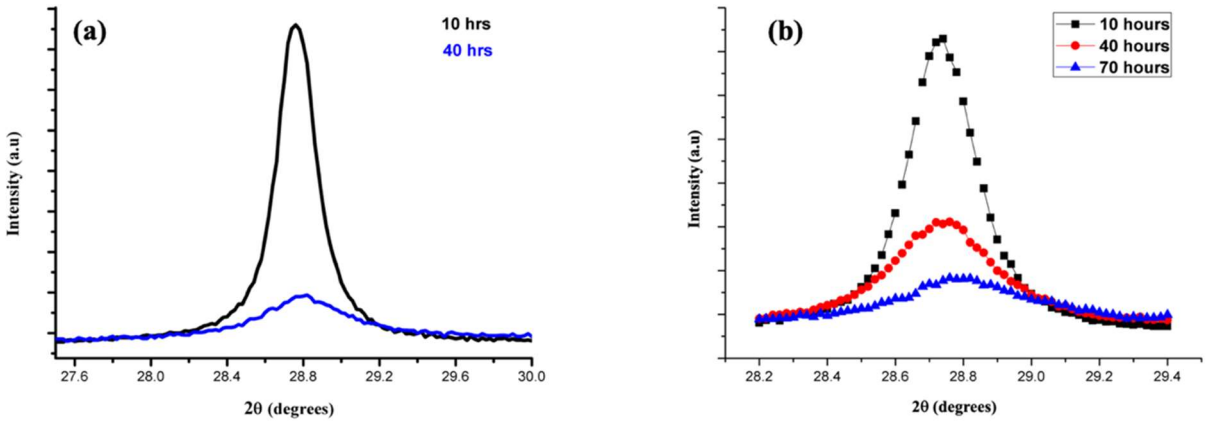

Figure 5.7: (a) The highest intensity (101) peak of (Ni/Mn)Sb showing the intensity profile for NiMnSb mechanically alloyed powders after 10 h and 40 h of alloying respectively (b)The highest intensity (101) peak of (Ni/Mn)Sb showing the intensity profile for NiMnSbV mechanically alloyed powders after 10 h, 40 h and 70 h of alloying respectively.

5.4.3 Role of atomic size and enthalpy of mixing

It has been widely reported in HEA/MEA literature that systematic substitution of elements in the crystal lattice leads to the formation of single-phase alloy with high configurational entropy. Similar concept has been extended to form high entropy intermetallic alloys [129]. It is understood that less difference in atomic size among the constituent elements would introduce minimal atomic scale strain in the lattice upon substitution. Additionally, negative binary enthalpy of mixing would favor atomic scale mixing of the elements in the lattice. It may be understood in the light of Hume-Rothery rule of solid solution formation, where similar crystal structure, less atomic size difference and small difference in electronegativity favors solid solution formation.

The NiMnSb and NiMnSbV alloys may be revisited in the light of the above discussion. Phase evolution and phase transformation in binary Ni-Mn system has been widely studied. The binary Ni-Mn phase diagram is complicated with a large number of intermetallic phases being present all through the composition range. In the equi-atomic NiMn alloy complex phase transformation from BCC to FCC to FCT [173] and finally ordering induced monoclinic phases are observed which is reported in chapter 3. However, addition of Sb, completely changes the phase to semi-Heusler NiMnSb.

Further the addition of V to NiMnSb alloy drastically changes the phase formation behavior again, leading to the formation of Frank-Kasper type SbV_3 phase in the matrix of semi-Heusler NiMnSb phase.

The atomic size mismatch and binary enthalpy of mixing between the constituent elements in the NiMnSb and NiMnSbV alloys are given in Table 4.1 and Table 4.2 respectively. It is observed from the Table 4.1 that atomic size mismatch values between Ni-Mn, Ni-Sb, Ni-V, Mn-Sb, Mn-V, Sb-V are 4%, 4.5%, 5%, 0.4%, 0.97%, 0.48% respectively. The binary enthalpy of mixing values as observed from the Table 4.2 are also negative to favor either solid-solution or intermetallic phase formation. However, under real experimental condition equi-atomic NiMn forms intermetallic phases, which shows structural complexity and a number of phase transformation over the temperature space. Addition of Sb, leads to the formation of only semi-Heusler NiMnSb intermetallic phase. Further addition of V, leads to the formation of a two-phase microstructure with one phase being Frank-Kasper type SbV_3 and the other phase being semi-Heusler NiMnSb. The phase formation is quite contrary to the commonly understood way of phase evolution in HEAs/MEAs based on atomic size mismatch and enthalpy of mixing. The authors would like to point out that total energy minimization is the main driving force in phase evolution. It is processing route dependent as the alloy may be kinetically held up in the energy landscape also. In estimating the total energy, higher order interactions among the constituent elements, other forms of entropy contribution should also be taken into account. Just binary enthalpy of mixing and atomic size mismatch may provide a rationale for the solid solution formation. However, it is crude and fails to predict accurately more often than not.

5.5 Conclusions:

The following conclusions can be made from the present work on NiMnSb and NiMnSbV MEAs:

i) Ordered hexagonal (Ni/Mn)Sb phase forms upon mechanical alloying for 10 h in equi-atomic NiMnSb and NiMnSbV alloys, which is destabilized on further mechanical alloying to form a disordered hexagonal solid solution phase along with amorphous phase.

ii) Kinetics of formation of disordered hexagonal solid solution phase along with the amorphous phase from the ordered hexagonal (Ni/Mn)Sb phase is faster in NiMnSb alloy than the NiMnSbV alloy.

iii) NiMnSb semi-Heusler phase forms in the as-solidified NiMnSb alloy. In as-solidified NiMnSbV alloy, along with the NiMnSb semi-Heusler phase, Frank-Kasper type SbV_3 phase also forms through solute rejection mechanism.

iv) Phase formation in NiMnSb and NiMnSbV alloys is synthesis route dependent as the phases formed through mechanical alloying are different from the phases formed through solidification.

v) Disordered hexagonal solid solution phase along with amorphous phase formation in NiMnSb and NiMnSbV alloys upon continued mechanical alloying may be attributed to the accumulation of strain in the lattice and increase in configurational entropy due to the presence of several elements.

vi) Systematic substitution in the lattice of semi-Heusler NiMnSb based on atomic radius mismatch and binary enthalpy of mixing is not the ideal way to design single-phase semi-Heusler based HEAs/MEAs.